Utilizing Response Surface Method for Optimization of the Removing Cu(II) Ions from Aqueous Solutions Using New Magnetic Chitosan-Based Nanocomposites Containing N-Nicotinyl Phosphoric Triamides

Rezaei Jamalabadi, Shahin; Oroujzadeh, Nasrin*+

Department of Chemical Technologies, Iranian Research Organization for Science and Technology (IROST), Tehran, I.R. IRAN

Abstract: *One of the newest methods to remove pollutants from water is the use of magnetic chitosan nanocomposites. Here for the first time, we used two phosphoramide compounds, N-Nicontinyl-N', N''-bis (piperidinyl) phosphoric triamide (P1) and N-Nicontinyl- N', N''-bis (4-methyl piperidinyl) phosphoric triamide (P2), in the structure of chitosan-based magnetic nanocomposites for the removal of Cu (II) ions from aqueous solution. The two chitosan/Fe_3O_4/ phosphoric triamide nanocomposites, NC1 and NC2, prepared using P1 and P2 respectively, were characterized using XRD, EDX, VSM, SEM, BET, and BJH methods. Removal of Cu (II) ions from polluted water was tested in different user conditions: pH (3-11), adsorbent dosages (5-25mg), and contact time of adsorbent with aqueous solutions (5-600 min). AAS (Atomic Absorption Spectroscopy) results showed that with increasing pH from 3 to 9, the amount of removal of Cu(II) ion increased, and with increasing pH from 9 to 11, the removal rate decreased. Heightening the contact time until 451 minutes also enhanced the removal efficiency up to 97.44%; After this time, the reduction of the removal amount was observed probably due to the desorption phenomena. Similarly, with the increasing amount of adsorbent (from 5 to 25 mg), the removal of Cu(II) ion increased too. Using Response Surface Modeling (RSM) the different conditions were transformed into RSM parameters and a second-order quadratic model was built to minimize the number of runs (36 runs) and also predict responses. A good correlation (with $R^2 = 0.9237$) was found between the experiment and the statistical model, for removing Cu(II) ions from the aqueous solution using these adsorbents.*

KEYWORDS: *Chitosan, Fe_3O_4, Nanocomposite, N-Nicotinyl Phosphoric triamde, Removal of Cu (II), Response Surface Method.*

INTRODUCTION

Currently, water is a highly important resource for humans and has far-reaching implications both environmentally, politically, socially, and economically across the globe. Due to its toxicity to human health, heavy

**To whom correspondence should be addressed.*

+ E-mail: n_oroujzadeh@irost.ir

1021-9986/2023/10/3278-3292 15/$/6.05

metal ions are subjected to extensive surveying and global restrictions are becoming ever more stringent [1, 2]. Copper is an essential element for the health and well-being of animals and plants, yet an excess of it can prove detrimental to all creatures. The overconsumption of copper can lead to a variety of health issues including headaches, liver diseases, heart irregularities, anemia and intestinal problems [3]. Activities such as metal melting, biocide application, and fungicide use involving copper can lead to water pollution [4]. Therefore, it is necessary to remove or reduce copper ions from contaminated drinking water and industrial wastewater output.

Recently, there has been considerable focus on employing chitosan nanocomposite derivatives for water purification purposes [5, 6]. Magnetic adsorption methods for wastewater treatment have gained substantial recognition in recent times, and are important to the process of separation [7–10]. The salient advantage of magnetic separation is that it facilitates the purification of a large amount of water in a short time span, with minimal energy investment and without compromising environmental quality [11]. Magnetic Chitosan Composites (MCC) containing a matrix of a dispersed phase including magnetic particles and chitosan polymer have attracted much attention in various fields including biomedicine, (drug delivery, artificial muscle, enzyme-based biofuel cells, bone regeneration) [12–15], environmental (contaminant removal, pollutant degradation) [16–19] and analytical applications such as (separation, biosensor, fluorescence probes, affinity chromatography) [20–23]. Also, MCCs have frequently been used in water treatment [24–26].

In addition to magnetic nanoparticles, numerous other compounds have been incorporated into the structure of magnetic chitosan nanocomposites, and their properties have been studied. For example, the effect of chitosan/ Fe_3O_4/ 2-aminopyridine glyoxal Schiff's base has been investigated on the removing of Ni(II), Cu(II), and Cd(II) [24]. Here, we have used two phosphoramidic compounds as novel additives in magnetic chitosan nanocomposites and studied them as adsorbents for Cu(II) ion removal. Phosphoric triamides are one of the most important classes of organophosphorus compounds that are utilized across many disciplines, including anticancer prodrugs, cholinesterase and butyrylcholinesterase inhibitors, pesticides, insecticides, catalysts of numerous chemical reactions and functional ligands in coordination chemistry. These compounds have drawn considerable attention due to their various noteworthy properties [27–38].

Given that most toxic metal ions are more readily adsorbed in acidic media and chitosan is soluble in low pHs, cross-linking agents such as glutaraldehyde [39], epichlorohydrin [40] and ethylene glycol diglycidyl ether [41] are often employed to reduce the dissolution of chitosan in acidic media. The cross-linking process provides an effective means of ensuring superior chemical and mechanical properties in the resultant chitosan [42,43].

Here, we prepared cross-linked magnetic chitosan\ N-Nicotinyl phosphoric triamide nanocomposites and used them to remove Cu(II) ions from an aqueous solution. Furthermore, different user conditions for adsorbent dosage, time, pH, and two types of adsorbent were optimized by RSM for optimal removal of Cu(II) ions.

EXPERIMENTAL SECTION

Chemicals and reagents

Phosphorus pentachloride, Ferric nitrate, Ferrous chloride tetrahydrate, 4-methyl piperidine, Piperidine, Carbon Tetrachloride, acetic acid, acetonitrile, distilled water, and starch obtained from Merck Co. High molecular weight chitosan was obtained from Loba Chemie Pvt. Ltd. Glutar aldehyde (25 wt% in water) was obtained from Daejong Co. Nicotinamide was obtained from Acros Co. All compounds were used without any further purification.

Synthesis

N- Nicotinyl phosphoric triamides

The N- Nicotinyl-N', N''-bis (piperidinyl) phosphoric triamide (P1) and The N- Nicotinyl-N', N''-bis (4-methyl piperidinyl) phosphoric triamide (P2) was synthesized based on the literature method [44]. Briefly, to a mixture of acetonitrile and N-Nicotinyl phosphoramidic dichloride (1 mmol), desired amine, piperidine for P1 and 4-methyl piperidine for P2, (4 mmol) was added at 0◦C. After 8 hours, the sediment obtained was filtered and washed with distilled water to obtain the final product, and dried at 25 °C.

Synthesis of Fe_3O_4 nanoparticles

The Fe_3O_4 magnetite nanoparticles were synthesized by a general procedure reported in the literature [45]

Table 1: The applied variables and design surfaces for each parameter

Type of variables	*Variables*	*surfaces*				
		+Alpha	+1	0	-1	-Alpha
	A: pH	11	9	7	5	3
Numerical	B: Contact time (min)	600	451.25	302.50	153.75	5
	C: Dosage of adsorbent (mg)	25	20	15	10	5
Categorical	D: Nanocomposite Structure	Nanocomposite Structure 1			Nanocomposite Structure 2	
		NC1			NC2	

A mixture of anhydrous $Fe(NO_3)_3$ (2 mmol) in ethanol and $FeCl_2{\cdot}4H_2O$ (1 mmol) plus 20 mmol of starch, was stirred for 1 hour at pH 8. Then, the obtained precipitate after washing with ethanol was dried in the vacuum [46].

Preparation of Chitosan/Fe_3O_4 NPs/Phosphoric triamide films

To the suspension containing 0.5 g of powder of chitosan in 5 ml of distilled water, 3 ml of acetic acid was added and the mixture for 2 hours was placed in an ultrasonic bath to obtain a homogeneous gel. Then a mixture of 0.05 g (10% weight of chitosan) N-Nicotinyl phosphoric triamide P1 or P2 with ethanol was added to the chitosan solution and placed for 30 minutes in the ultrasonic bath. Next, 0.25g (5% weight of chitosan) of Fe_3O_4 NPs was added to the mixture and placed again in the ultrasonic bath for another 30 min. Following this, the mixture was sonicated by an ultrasonic probe to effectively distribute the nanoparticles and phosphoric triamide compounds within the chitosan framework. Films were prepared by drying the mixture in a Petri dish then left in a desiccator with glutaraldehyde vapor at 0.5 atm for a period of 24 hours to complete the chitosan cross-linking process. Afterward, the product films were washed with ethanol, acetic acid and distilled water consecutively to remove uncrosslinked chitosan and any remaining unreacted glutaraldehyde before being dried at room temperature.

Characterization of the adsorbents

The surface morphology of the NC1 and NC2 was investigated with Scanning Electron Microscopy (SEM, Mira II, Tescan Co.). The elemental analysis of the prepared nanocomposite films was determined by Energy-Dispersive X-ray spectroscopy. (EDX, Mira II, Tescan Co.). The specific surface, pore volume, and pore size of the adsorbents were determined using Brunauer, Emmett, and Teller (BET) method (ASAP 2020 M+C, Micromeritics, Co.). Phase analysis of the fabricated framework was carried out by X-ray diffraction (XRD) (Model: Equinox 3000, Intel Co.). Using a vibrating sample magnetometer (VSM, Model: 7407, Lake Shore Co.), the magnetic behavior of Fe_3O_4 nanoparticles, NC1 and NC2 was investigated.

Cu(II) ions removal

First, 20 ml of a Cu solution with 100 mg/L concentration, was prepared by dissolving $Cu(NO_3)_2$ in distilled water in all cases. The pH of the solution was adjusted by using HNO_3 and NH_3, both with the concentration of 0.1 M. As stated by the adsorption design matrix of variables in Table 1, two adsorbents (NC1 and NC2) were used with different doses (5-25 mg) for different solutions at different times (5-600 minutes) and pH (11-3). The samples were stirred on a thermostatically-controlled stirrer at 25 °C and 150 rpm. Following each run, solid phase was separated by means of a magnet and the adsorption of Cu(II) ions for each sample was analyzed using atomic absorption spectroscopy (Model: AAS-240-Varian Co.).

To calculate the removal efficiency of Cu(II) ions, the difference between the initial and residual concentrations was used to determine the percentage of removed Cu(II) ions using the following equation [47]:

$$R\% = \frac{(C_i - C_e)}{C_i} \times 100 \quad (1)$$

$$q_e = \frac{C_i - C_e}{m} \times V \quad (2)$$

Where C_e (mg/L) is the equilibrium concentration (After removal) and C_i (mg/L) is the initial concentration. In Equation (2) which considers the adsorption process: V is the solution volume (L), q_e (mg/g) is the adsorption capacity, and m is the adsorbent mass (g).

The equilibrium value of the adsorption process can be expressed through the distribution of Cu(II) between the adsorbent and liquid phase, which can be evaluated

using isotherm models. In this study, equilibrium data for two-parameter isotherm models was used, specifically Langmuir [48] and Freundlich [49]. The Freundlich and Langmuir isotherms were utilized to analyze the Cu(II) removal using magnetic chitosan nanocomposites.

Langmuir: $\frac{C_e}{q_e} = \frac{1}{q_{max} K_L} + \frac{C_e}{q_{max}}$ (3)

Freundlich: $\log q_e = \log K_F + \left(\frac{1}{n}\right) \log C_e$ (4)

Where K_L (L/mg) is the Langmuir constant related to the monolayer adsorption capacity and the adsorption's free energy ($K_L=e^{-\Delta G/RT}$). K_F (L/mg) is the Freundlich constant related to sorption capacity, q_{max} (mg/g) is the maximum adsorption capacity and n is the heterogeneity factor. The constants for the Freundlich and Langmuir models for linear regression were obtained from plotting (i) (C_e/q_e) versus C_e and (ii) log q_e against log C_e.

Response surface modeling

Response Surface Modeling (RSM) is a practical statistical approach that utilizes quantifiable data derived from scientifically designed experiments to optimize a regression model and adjust its operational parameters [50]. The primary goals of RSM are to devise the experimental layout for a process and to ascertain the best set of operational variables for it [51]. The design of an adsorption process experimentally can decrease processing time, variability, and total expenses while attaining improved process output [52]. The RSM approach has been widely utilized in chemical engineering and optimization of sorption processes [53]. The Central Composite Design (CCD) method has been extensively utilized to develop a second-order model and requires a minimal amount of experiments to be conducted. The response surface modeling technique helps to analyze the reaction of total variables space and to identify the region where it attains its optimal value.

According to Table 1, three parameters (time, pH, and adsorbent dosage) were chosen for the two nanocomposites. Afterwards, Design Expert 7.0 was utilized in order to perform regression analysis and determine the constants of the response model [51]. The relationship between the response of the process and the three independent variables is modeled by a quadratic equation [54].

$$Y = a_0 + \sum_{j=1}^{n} a_j X_j + \sum_{j=1}^{n} a_{jj} X_j^2 + \sum_{i}^{n} \sum_{j=1}^{n} a_{ji} X_j X_i \quad (5)$$

Here Y is the response coefficient for Cu(II) removal, a_0 is the intercept term, X_i and X_j are variables, a_i is a factor that defines the effect of the parameter (i) in the response for the linear term, and, a_{ij} refers to the interaction effect between the i and j variables and a_{ii} can be considered as the shape parameter of the curve (quadratic effect).

The integrity of fit of the model equation is estimated by Adjusted R^2 and R^2. The Adjusted R^2 modifies the R^2 value for the amount of samples and number of terms in the model [53].

In order to optimize the three variables of this study, 36 experiments were designed using Design Expert 7.0. The matrix related to the residual concentrations of Cu(II) and the design as a response is presented in Table 2. The performance of the method is quantified through a quadratic equation:

$Y= (Cu\ Removal) = 8.98 + 0.97A + 0.082B + 0.25C + 0.14D – 0.69A^2 – 0.14B^2 + 0.061C^2$

Where A, B, C and, D are respectively pH, time, adsorbent dosage and the type of nanocomposite.

RESULTS AND DISCUSSION

Characterization of chitosan/Fe_3O_4/phosphoric triamide nanocomposites

X-Ray diffraction (XRD) analysis

For the approval of the presence of Fe_3O_4 nanoparticles and phosphoric triamide compounds in nanocomposite frameworks, the structure of the chitosan, phosphoric triamide, and magnetic nanocomposite was indicated by XRD and the diffractograms was shown in Figs. 1 and 2. Characteristic diffraction peaks of Fe_3O_4 in the XRD graph of nanocomposite films, based on the standard cards can be indexed as (220), (311), (400), (422), and (333) planes [55]. As it can be seen in Figs. 1 and 2, the mixing process did not cause any phase change in Fe_3O_4 MNPs and other components of the nanocomposites.

The utilization of ultrasonic waves in the mixing process has caused a variance in the intensity of some phosphoric triamide selections. While there is minimal effect of scattering on the structures of phosphoric triamide and magnetic particles, one noticable exception is that the amorphous phase of chitosan appears as the major source

Table 2: Design matrix of three variables in actual and coded forms along with observed response

Run	pH	Contact time (min)	Adsorbent dosage (mg)	Type of Nanocomposite	Removal efficiency (%)	Predicted Removal efficiency (%)
1	7	302.5	15	NC1	74.2	78.03
2	3	302.5	15	NC1	17.68	16.65
3	7	302.5	5	NC1	69.91	71.27
4	9	451.25	10	NC1	85.17	76.6
5	5	451.25	10	NC1	49.21	50.22
6	7	5	15	NC1	59.62	61.35
7	9	451.25	20	NC1	95.67	88.12
8	11	302.5	15	NC1	58.68	70.69
9	7	600	15	NC1	67.14	68.23
10	5	153.75	20	NC1	55.52	56.06
11	9	153.75	10	NC1	81.31	73.28
12	7	302.5	15	NC1	77.29	78.03
13	7	302.5	25	NC1	88.84	91.11
14	5	153.75	10	NC1	47.02	47.74
15	9	153.75	20	NC1	95.34	83.72
16	5	451.25	20	NC1	59.7	59.62
17	7	302.5	15	NC1	79.19	78.03
18	7	302.5	15	NC1	76.17	78.03
19	5	451.25	10	NC2	53.21	54.78
20	5	153.75	10	NC2	52.63	53.18
21	5	451.25	20	NC2	62.39	62.42
22	7	600	15	NC2	71.14	71.69
23	7	302.5	15	NC2	86.9	82.37
24	5	153.75	20	NC2	56.13	59.74
25	7	302.5	5	NC2	73.37	77.37
26	7	302.5	25	NC2	89.9	93.69
27	7	5	15	NC2	67.54	66.57
28	9	153.75	10	NC2	89.45	79.16
29	11	302.5	15	NC2	58.91	75.47
30	9	451.25	20	NC2	97.44	91.36
31	9	153.75	20	NC2	97.13	87.84
32	7	302.5	15	NC2	81.88	82.37
33	9	451.25	10	NC2	91.56	81.6
34	3	302.5	15	NC2	18.66	20.55
35	7	302.5	15	NC2	88.37	82.37
36	7	302.5	15	NC2	83.22	82.37

of scattering in Figs. 1(a) and 2(a). Due to the high crystallinity of the phosphoric triamide component of the nanocomposite, sharp peak patterns of phosphoric triamide are observed [56] (Fig. 1b and 2b), While chitosan shows only one wide particular peak at 2Θabout 20◦ because of its amorphous polymeric structure (Fig. 1c and 2c). The Full Width at Half-Maximum (FWHM) of each 2Θ position for phosphoric triamide used in the Debye–Scherrer equation to calculate the average crystallite size is determined ($d = 0.9\lambda/\beta\cos\Theta$) [57], where (λ) is

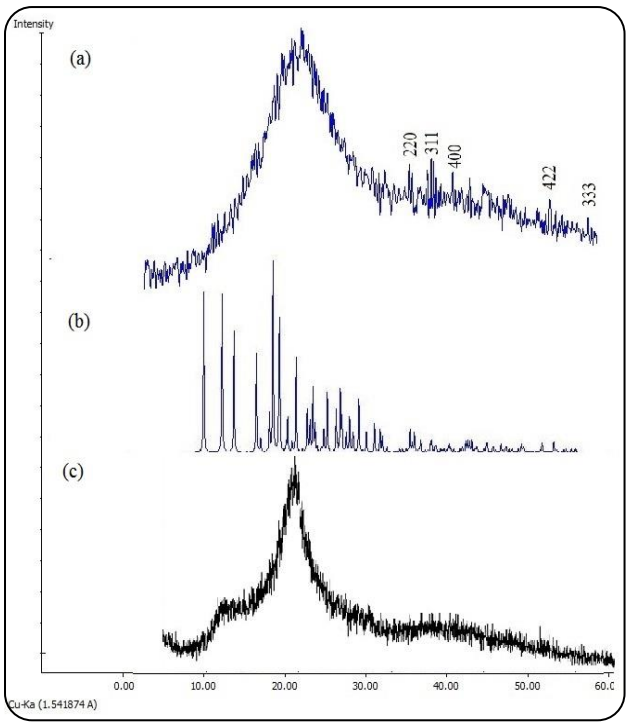

Fig1: XRD patterns of NC1 (a), P1 (b) and Chitosan (c)

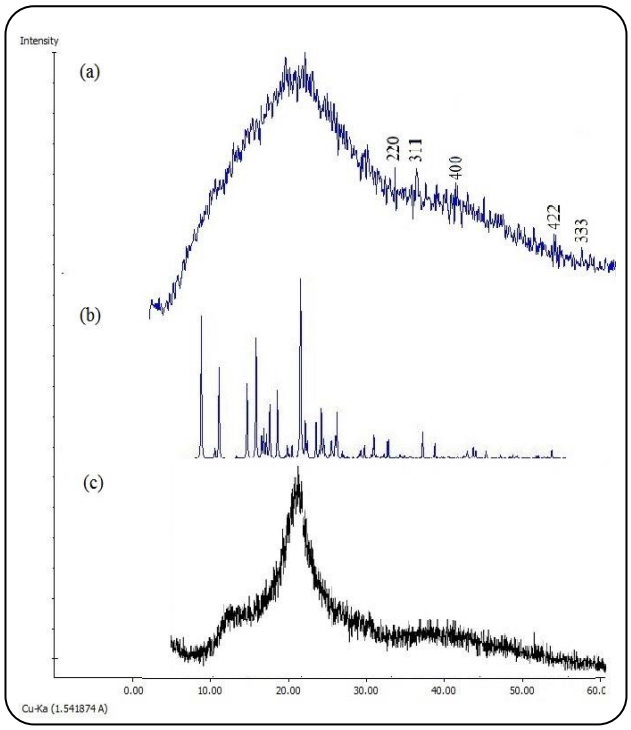

Fig2: XRD patterns of NC2 (a), P2 (b) and Chitosan (c)

the wavelength of the X-ray, (β) is the full width at half maximum or FWHM, (Θ) is the diffraction angle and (d) is the average crystallite size. From the above equation, the average crystal size was obtained as 39.10 nm for P1 and 40.11 nm for P2.

FE-SEM micrographs, EDX and BET

Field Emission Scanning Electron Microscopy (FE-SEM) and EDX was used to investigate the morphology of the surface, estimating the particle sizes and assuring the elemental analysis of the cross-linked Fe_3O_4/Chitosan/N-Nicotinyl phosphoric triamide nanocomposite films (Fig. 3 and 4). As illustrated in Fig. 3, the nanoparticles are visible in the structure of the nanocomposites, and an optimal dispersion of the components can be seen at the surface of the products. EDX results clearly showed that the phosphoric triamide compound and Fe_3O_4 nanoparticles were correctly supported on the framework of chitosan (Fig. 4).

Utilizing the Brunauer–Emmett–Teller (BET), the pore size, specific surface area, and the total pore volume of NC1 and NC2 were also defined in Table 3. Results showed that NC2 has more suitable surface properties for adsorbing Cu (II) ions than those for NC1.

VSM analysis

The Fe_3O_4 nanoparticles and the prepared nanocomposites (NC1 and NC2) magnetic hysteresis loops are shown in Fig. 5. As can be seen from the hysteresis loops, regarding the magnetic saturation scale, Fe_3O_4 NPs show a super-paramagnetic behavior and as-prepared nanocomposites, NC1 and NC2 have a paramagnetic manner. This means that these nanocomposites as magnetic adsorbents can be deemed as cost-effective water purifiers easily removed by a magnetic field after removing Cu(II) ions.

The measured saturation magnetism for Fe_3O_4 NPs, NC1, and NC2, were 63.37, 1.72, and 1.89 emu/g respectively. The lower magnetic value for NC1, and NC2 compared with naked Fe_3O_4 nanoparticles, which has been reported for similar magnetic nanocomposites, could be due to the coverage of magnetic Fe_3O_4 NPs by the matrix of non-magnetic components (here: chitosan and phosphoric triamide) [58].

Adsorption isotherms

To optimize the parameters of the adsorption process, Langmuir and Freundlich models of isotherm were used for the analysis of experimental data. Langmuir model can be used for monolayer adsorption on surfaces with

Table 3: Nanocomposites Porosimetry data of BET

	Specific surface area (m^2/g)	Pore size (nm)	total pore volume (cm^3/g)
NC1	1.778	7.914	0.178
NC2	2.828	14.542	0.649

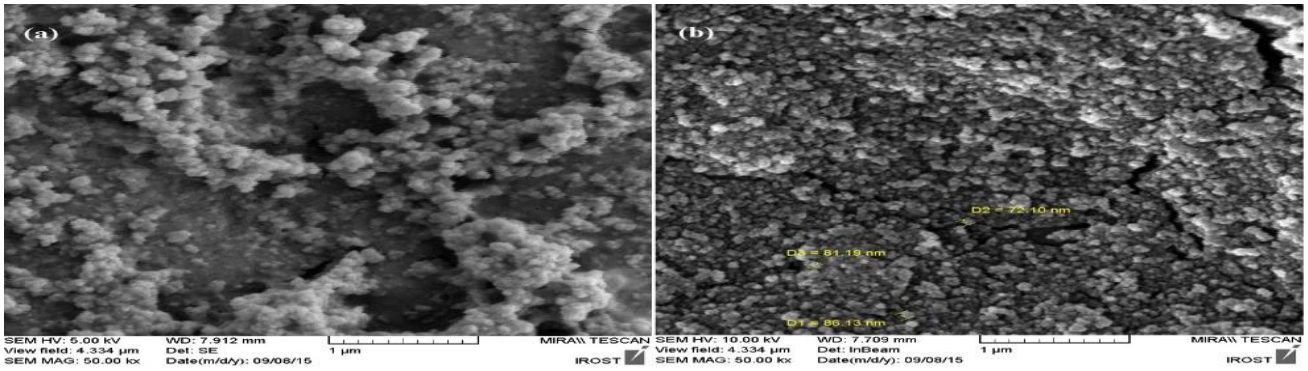

Fig3: The FE-SEM micrograph of NC1 (a), NC2 (b)

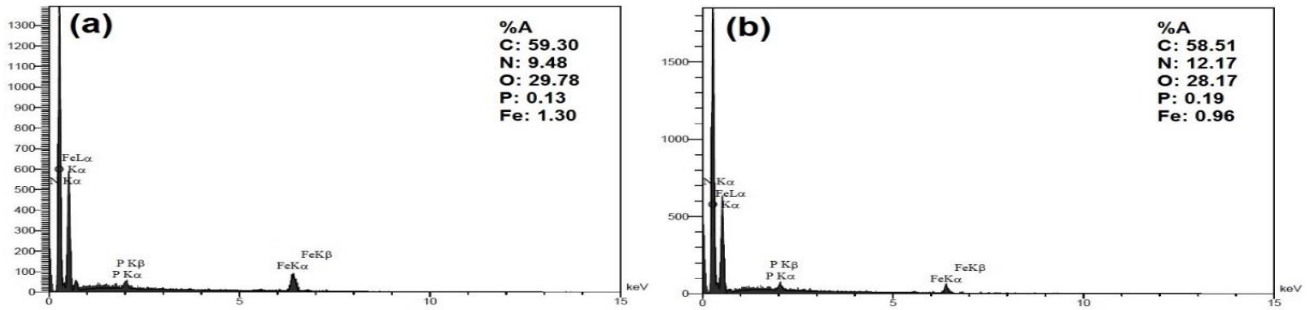

Fig4: The EDX analysis of NC1 (a), NC2 (b

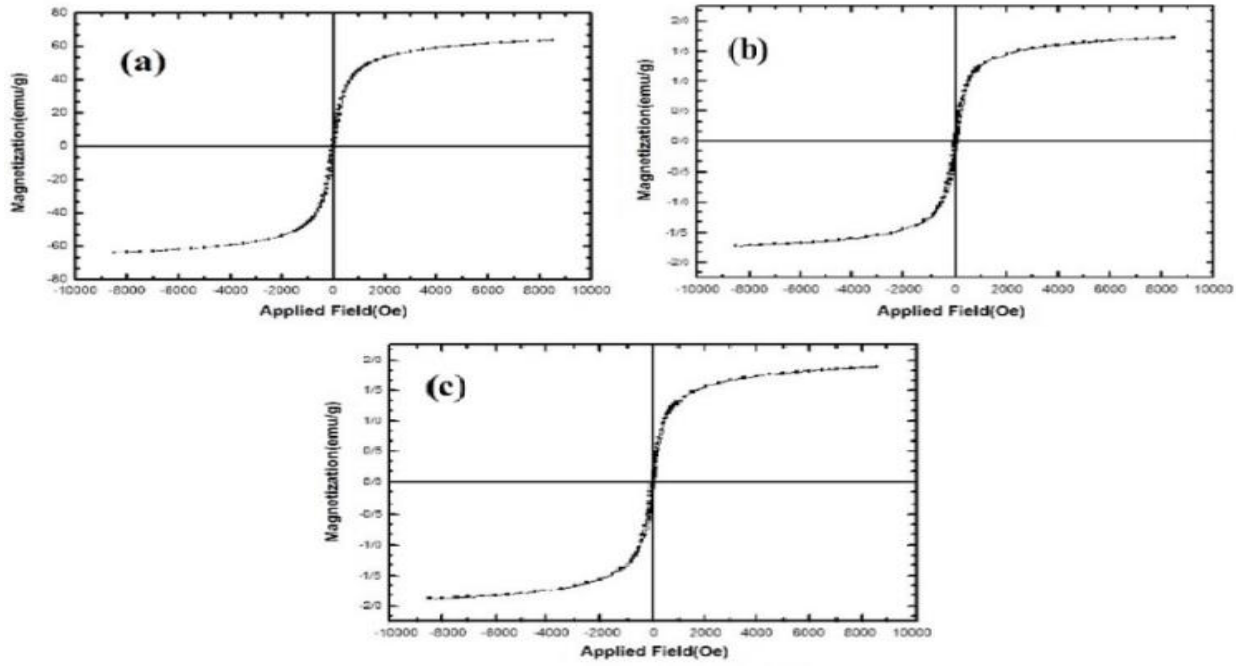

Fig 5: Magnetic hysteresis loops of Fe_3O_4 nanoparticles (a), NC1 (b) and NC2 (c)

Table 4: Parameters of adsorption isotherms for Cu(II) adsorption on NC1 and NC2

Isotherm	Equation		Value of parameters	Adsorbents	
				NC1	NC2
Langmuir	$\frac{C_e}{q_e} = \frac{1}{q_{max}K_L} + \frac{C_e}{q_{max}}$	The constants q_{max} and K_L are calculated by the plot of C_e/q_e versus C_e with slope $1/q_{max}$ and intercept $1/(q_{max}.K_L)$	q_{max} (mg/g)	113	113.21
			K_L (l/mg)	737965.91	453698.2
			R^2	0.995	0.995
Freundlich	$\log q_e = \log K_F + \left(\frac{1}{n}\right)\log C_e$	K_F and n can be calculated from a linear plot of $\log q_e$ against $\log C_e$	1/n	0.142	0.3005
			K_F (l/mg)	151.63	310.64
			R^2	0.9963	0.998

Table 5: Comparison of various adsorbents used for Cu(II) removal from aqueous solutions

Adsorbent	Optimum pH	Temp. (K)	Adsorption capacity (mg/g)	Removal efficiency %	Ref.
NC1	9	298	113	95.67	This study
NC2	9	298	113.21	97.44	This study
Poly-acrylamide	10 - 11.5	298	123.6	95	[64]
Poly-ferric sulfate	10 – 11.5	298	82.4	99.6	[64]
CTABr	8 - 10	298	200	99.9	[65]
Zeolite	8 - 10	298	200	97	[66]
chitosan-enhanced membrane filtration	8.5 – 9.5	298	NA	95	[67]
Polyamide	4 - 11	298	NA	98	[68]
$Mg(OH)_2$	9.5	298	NA	80	[69]
Formaldehyde cross-linked modified chitosan–thio glyceraldehyde Schiff's base	5	303	76	58	[70]
Xanthate-modified magnetic chitosan	5	298	34.5	NA	[71]
Cross-linked magnetic chitosan beads	6	298	78.13	NA	[72]
Uniform magnetic chitosan microcapsules	7	303	104	NA	[73]
Chitosan-coated magnetic nanoparticles modified with α-ketoglutaric acid	6	295	96.15	NA	[74]
Magnetic chelating resin based on chitosan	5	301	95	NA	[75]
Thiourea-modified magnetic ion-imprinted chitosan/TiO_2 composite	5.5	303	174	NA	[8]
Fly ash-based linde F (K) Zeolite	7	318	23.4	NA	[76]
Riverbed Sand	8	298	7.93	NA	[77]
Sodium iodate cork biomass	10	298	19	NA	[٧٨]

NA: Not Available

a limited number of identical sites of adsorption [48]. The Freundlich Isotherm is an earlier experimental equation that is reliable with an exponential dispersion of active sites and assumes adsorption of metal ions occuring on the heterogenous surface of the adsorbent [49]. In Table 4, the linear form of Langmuir and Freundlich isotherm models is shown.

The constants of the Langmuir and Freundlich isotherms, as well as the coefficients of the correlations with this research's experimental data, are displayed in Table 5. The coefficient of correlation, (R^2), is higher for Freundlich isotherm compared to Langmuir isotherm. Also, Maximum adsorption capacity (q_{max}) calculated, and it was 113 mg/g for NC1 and 113.21 mg/g for NC2. The (n) value obtained from the Freundlich isotherm was >3.3, which is bigger than 1.0, informing a high affinity between the adsorbent and adsorbate [59].

Performance evaluations

Table 5 shows the comparison of maximum absorption capacities (q_{max}) for Cu(II) using NC1 and NC2 with other results reported in the literature. It is observed that the maximum absorption capacity of Cu(II) for NC1 and NC2 is higher than most other materials, which is due to the strong adsorption capacity of NC1 and NC2.

Table 6: Analysis of variance results (ANOVA) for quadratic model used for Cu(II) adsorption

Source of variation	Sum of Squares	DF	Mean square	F-value	P-value Prob > F
Model	12661	13	973.92	20.48	< 0.0001
A-pH	6605	1	6605	138.89	< 0.0001
B-Time	57	1	57	1.21	0.2838
C-Dosage	618	1	618	13	0.0016
D-NC	186	1	186	3.91	0.0608
A^2	4513	1	4513	94.91	<0.0001
B^2	454	1	454	9.55	0.0053
C^2	4.90	1	4.90	0.1	0.7512
Residual	1046	22	47.56		
Lack of fit	1005	16	62.84	9.21	0.0058
Pure Error	40.91	6	6.82		
Cor Total	13707	35			

R^2 = 0.9237, CV = 9.71%, Adjusted R^2= 0.8786, Predicted R^2= 0.7484, DF: Degree of freedom.

It is evident that Cu(II) ions can be removed from aqueous solutions across a broad pH range using various chemical modification agents depending on the removal process, agent utilized, and pH of the medium. As illustrated in Figs. 7 and 10, the optimal removal pH for NC1 and NC2 is pH 9. By increasing the pH from 9 to 11, some Cu(II) ions precipitate in the forms of $Cu(OH)_4^{2-}$, $Cu(OH)_3^-$, and $Cu(OH)_2$ [60]. Thus, the amount of Cu(II) ions in the aqueous solution decreases and the active sites on the adsorbent's surface become occupied by $Cu(OH)_3^-$, $Cu(OH)_2$, and $Cu(OH)_4^{2-}$ species, which according to their sizes can occupy more spaces of nanocomposites' active sites. The decrease in removal efficiency of Cu(II) ions at pH levels higher than 9 is caused by these two phenomena [52]. In other words, the decrease in copper removal rate for solutions with a pH above 9 is due to the competition between the active sites of adsorbent surface networks for adsorption of Cu(II) ions and hydroxide ions in solution [61, 62]. This state forms a MOH bond (M is a metal such as Cu) that chelates metal ions in solution, thereby limiting the transfer of metal ions to the active sites of the adsorbent and decreasing the adsorption percentage [63].

Removal of Cu(II) ions

The results of the analysis of variance for the quadratic model used for Cu(II) ion adsorption obtained from RSM, as presented in Table 6, demonstrate a very close agreement between experiment and software's data prediction with both R^2 and "Adjusted R^2" values near 1. The associated Prob>F value for the quadratic model is also less than 0.0001, which indicates that the model is statistically significant for the response and thus suitable to be used in further analysis [79].

The value of R^2 indicates how much of the variation in the data is accounted for by the model [80]. R^2 coefficient, from the quadratic regression model, was determined with a value of 0.9237. This means that 92.37% of the variation for Cu(II) removal efficiency is defined by the independent variables, and this means that only about 7.63% of the variation is not explained by this model. Additionally, Adjusted R^2 is a measure of model fit that modifies the value of R^2 by taking into account the number of predictors or covariates present in the model. Here, the value of Adjusted R^2 (0.8786) is very near to the corresponding R^2 value. The high R^2 coefficient values indicate a satisfactory fit of the quadratic model to the experimental data [81]. Concurrently, in this research, the low value for the coefficient of variation percentage (C.V.%) (9.71%) is in the sufficient range (0.5–13.5%) [60, 61]. Also, this value implies that the change in the average value is satisfactory and acceptable [82], [83]. The "Lack of Fit F-value" of 9.21 implies that the Lack of Fit value is in acceptable range. There is just 0.58% chance that "Lack of Fit F-value" happened is out of noise. Also, the "Predicted R^2" of 0.7484 is in acceptable agreement with "Adjusted R^2" of 0.8786.

The comparison between the experimental values and the predicted values of the Cu(II) removal efficiency is illustrated in Fig. 6. All the data points are closely aligned with the scatter regression line, confirming that the predicted values are in agreement with the experimental values [79].

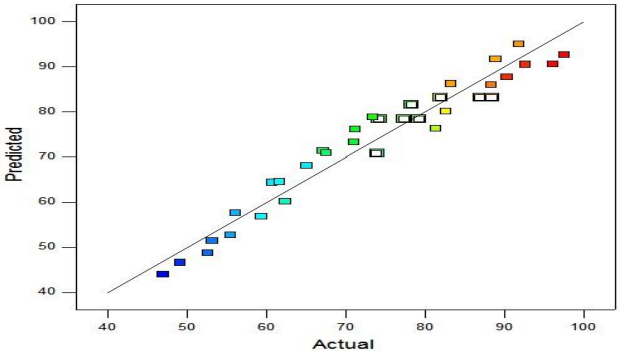

Fig.6: plot of predicted vs. experimental values for Cu (II) removal efficiency

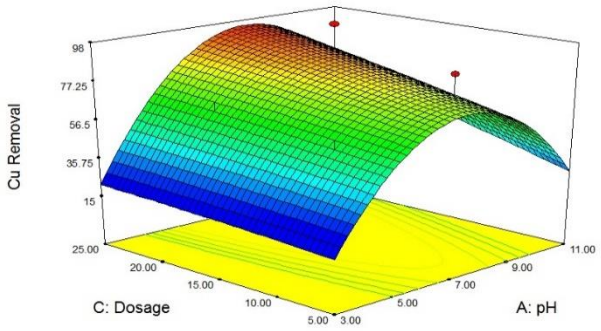

Fig. 7: 3D graph of interaction effect between pH and dosage of adsorbent at the Cu(II) removal level

Estimation of the variables effect on the Cu(II) ions removal by RSM

As evidenced by Table 6, Cu(II) adsorption capacity has generally been increased with the addition of N-Nicotinyl phosphoric triamide to the nanocomposite. This improvement can be attributed to the functional groups of the phosphoric triamides, including the amine group, which have been discussed previously in various publications [24], [45]. As shown in Table 6, the incorporation of N-Nicotinyl phosphoric triamide into nanocomposite altered the behavior of magnetic chitosan nanocomposite, with optimum pH being reached in an alkaline medium. Furthermore, the adsorption capacity increased compared to that of magnetic chitosan composite without N-Nicotinyl phosphoric triamide, which suggests that this additional compound is capable of enhancing Cu(II) ions removal efficiency. One of the critical elements for absorption is the pH of the aqueous solution, as this affects the connectivity of Cu(II) ions to adsorbents' functional groups. Numerous studies have examined pH's effect on the removal of Cu(II) ions with various adsorbents from both acid and alkaline solutions in a range from 2 to 9 [84]. In this study, it was observed that the removal of Cu(II) ions increased with an increase in pH up to pH = 9. Since the two prepared nanocomposites contain different functional groups such as OH, NH, NH_2, and O=P, altering the pH of the solution will alter these functional groups' behavior. In low pH, most of the functional groups in the nanocomposite are protonated and present in their positive charge form. Also, H^+ and H_3O^+ ions, which a large amount of it exist in an acidic solution, and due to the competition with Cu(II) ions for absorption in the existing areas of the nanocomposite, it can reduce the amount of Cu(II) ions absorption in acidic media. As a result, electrostatic repulsion between the positively charged nanocomposite surface and Cu(II) ions leads to reduced adsorption at very low pH [17].

Fig. 7 illustrates the 3D graph of the relationship between adsorbent dose and pH in the adsorption process. As can be seen from Figs. 7 and 10, the percentage of Cu(II) removal is enhanced with an increase in pH (from 3 to 9), but decreases when pH is elevated above 9. By increasing the pH from 9 to 11, some Cu(II) ions precipitate in form of $Cu(OH)_4^{2-}$, $Cu(OH)_3^-$, and $Cu(OH)_2$ [60]. As the amount of Cu(II) ions in solution decreases, the active sites on the surface of the adsorbent become covered by $Cu(OH)_4^{2-}$, $Cu(OH)_3^-$, and $Cu(OH)_2$ species, According to their sizes, larger molecules can occupy more active sites of nanocomposites, leading to decreased efficiency of Cu(II) ions removal at pH values above 9 [52].

The quantity of adsorbent utilized in the metal adsorption process is a considerable factor. Optimizing the amount of adsorbent is a significant matter when it comes to decreasing the cost of the process and minimizing pollution [63]. In Fig. 8, the 3D plot displays the interaction effect between contact time and adsorbent dosage on Cu(II) removal level. As can be seen from this graph, when the adsorbent dosage is increased (from 5 to 25 mg), there is a considerable increase in the rate of Cu(II) ions removal. Additionally, due to the presence of active sites on the adsorbent, an increase in adsorbent dosage also leads to an enhanced adsorption efficiency [85].

Fig. 9 illustrates a 3D plot depicting the effect of pH and contact time on Cu(II) ion removal. Figs. 9 and 11 demonstrate that, as contact time increases, removal efficiency slightly decreases. This may be explained by the reduction

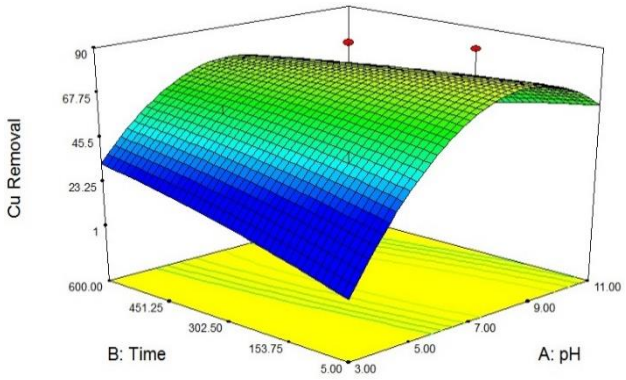

Fig. 9: 3D graph of interaction effect between contact time and pH at the Cu(II) removal level

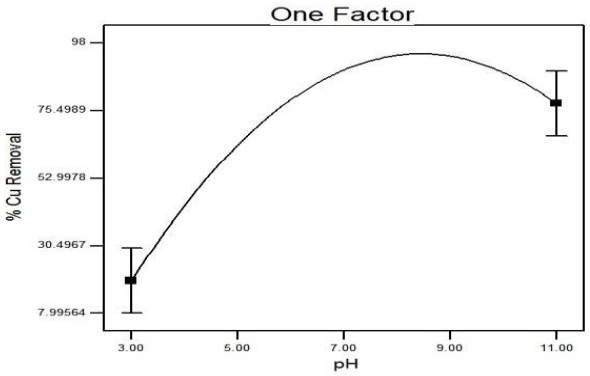

Fig. 10:One Factor estimation graph for pH effect at the Cu(II) removal level

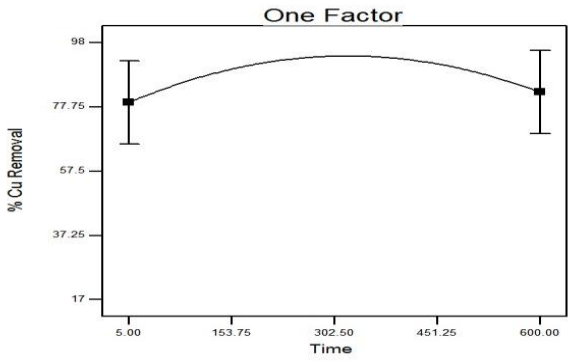

Fig. 11: One Factor estimation graph for contact time effect at the Cu(II) removal level

in adsorption surface area that occurs when contact time is prolonged; this could be caused by either the removal of Cu(II) ions from the adsorbent surface or from the concentration of Cu(II) ions in solution [86]. At higher sorbent doses, it is possible to experience partial overlap, as there are fewer active surfaces [74,79,80].

CONCLUSIONS

In this study, two new magnetic chitosan/ N-nicotinyl phosphoric triamide nanocomposite films were developed to efficiently remove Cu(II) ions from contaminated aqueous solutions. The Response Surface Methodology (RSM) was used to estimate the optimal conditions for removing this heavy metal ion from aqueous solutions. Moreover, the removal rate of Cu(II) from aqueous solution by the prepared nanofilms was studied in different user conditions.

According to the obtained results, for NC1, in the optimal condition when 20 mg of adsorbent is in contact at pH 9 for 451.25 minutes, it can remove 95.67% of Cu(II) from the aqueous solution and the optimal condition for NC2 is the same as NC1 with the removal of 97.44% of Cu(II) from the aqueous solution.

Acknowledgements

This project was funded by the Iranian Research Organization for Science and Technology.

Received : Apr. 10, 2023 ; Accepted : Jul. 12, 2023

REFERENCES

[1] Savenije H.H.G., Why Water Is not an Ordinary Economic Good, or Why the Girl is Special, *Phys. Chem. Earth, Parts A/B/C*, **27(11):** 741–744 (2002).

[2] Aguilera-Klink F., érez-MorianaE. P., Sánchez-Garcıa J., The Social Construction of Scarcity. The Case of Water in Tenerife (Canary Islands), *Ecol. Econ.*, **34**: 2 233–245 (2000).

[3] Kinson K., Belcher C.B., The Determination of Minor Amounts of Copper in Iron and Steel by Atomic Absorption Spectrophotometry, *Anal. Chim. Acta*, **31**: 180–183 (1964).

[4] Xu J., Yang L., Wang Z., Dong G., Huang J., Wang Y., Toxicity of Copper on Rice Growth and Accumulation of Copper in Rice Grain in Copper Contaminated Soil, *Chemosphere*, **62(4):** 602–607, 2006.

[5] Bhatnagar A., Sillanpää M., Utilization of Agro-Industrial and Municipal Waste Materials as Potential Adsorbents for Water Treatment—a Review, *Chem. Eng. J.*, **157(2)**: 277–296 (2010).

[6] Bhatnagar A., Kumar E., Sillanpää M., Fluoride Removal from Water by Adsorption—A Review, *Chem. Eng. J.*, **171(3)**: 811–840, 2011.

[7] Yavuz C.T., Prakash A., Mayo J.T., Colvin V.L., Magnetic Separations: From Steel Plants to Biotechnology, *Chem. Eng. Sci.*, **64(1)**: 2510–2521 (2009).

[8] Chen A., *et al.*, Novel Thiourea-Modified Magnetic Ion-Imprinted Chitosan/TiO_2 Composite for Simultaneous Removal of Cadmium and 2, 4-Dichlorophenol, *Chem. Eng. J.*, **191**: 85–94 (2012).

[9] Li H., Bi S., Liu L., Dong W., Wang X., Separation and Accumulation of Cu(II), Zn(II) and Cr(VI) from Aqueous Solution by Magnetic Chitosan Modified with diethylenetriamine, *Desalination*, **278(1):** 397–404 (2011).

[10] Wang Y., Li L., Luo C., Wang X., Duan H., Removal of Pb^{2+} from Water Environment Using a Novel Magnetic Chitosan/Graphene Oxide Imprinted Pb^{2+}, *Int. J. Biol. Macromol.*, **86**: 505–511 (2016).

[11] Feng Y., *et al.*, Adsorption of Cd (II) and Zn (II) from aqueous Solutions Using Magnetic Hydroxyapatite Nanoparticles as Adsorbents, *Chem. Eng. J.*, **162(2)**: 487–494 (2010).

[12] Qu J.-B., Shao H.-H., Jing G.-L., Huang F., PEG-Chitosan-Coated Iron Oxide Nanoparticles with High Saturated Magnetization as Carriers of 10-Hydroxycamptothecin: Preparation, Characterization and Cytotoxicity Studies, *Colloids Surfaces B Biointerfaces*, **102**: 37–44 (2013).

[13] Ashokkumar M., Sumukh K.M., Murali R., Narayanan N.T., Ajayan P.M., Thanikaivelan P., Collagen–Chitosan Biocomposites Produced Using Nanocarbons Derived from Goatskin Waste, *Carbon*, **15**: 5574–5582 (2012).

[14] Chung E.-Y., *et al.*, Design of Deformable Chitosan Microspheres Loaded with Superparamagnetic Iron Oxide Nanoparticles for Embolotherapy Detectable by Magnetic Resonance Imaging, *Carbohydr. Polym.*, **90(4)**: 1725–1731 (2012).

[15] Lee H. U., Song Y.S., Suh Y. ., Park C., Kim S.W., Synthesis and Characterization of Glucose Oxidase–Core/Shell Magnetic Nanoparticle Complexes into Chitosan Bead, *J. Mol. Catal. B Enzym.*, **81**: 31–36, (2012).

[16] Yang G., *et al.*, Cd (II) Removal from Aqueous Solution by Adsorption on α-Ketoglutaric Acid-Modified Magnetic Chitosan, *Appl. Surf. Sci.*, **292**: 710–716 (2014).

[17] Reddy D.H.K. Lee S.-M., Application of Magnetic Chitosan Composites for the Removal of Toxic Metal and Dyes from Aqueous Solutions, *Adv. Colloid Interface Sci.*, **201**: 68–93 (2013).

[18] Shen C., Shen Y., Wen Y., Wang H., Liu W., Fast and Highly Efficient Removal of Dyes under Alkaline Conditions Using Magnetic Chitosan-Fe (III) Hydrogel, *Water Res.*, **45(16)**: 5200–5210 (2011).

[19] Naghizadeh A., Ghafouri M., Synthesis of Low-Cost Nanochitosan from Persian Gulf Shrimp Shell for Efficient Removal of Reactive Blue 29 (RB29) Dye from Aqueous Solution, *Iran. J. Chem. Chem. Eng.(IJCCE)*, **38(6)**: 93–103 (2019).

[20] J Li., Y Zhang., Shen F., Yang Y., Comparison of Magnetic Carboxymethyl Chitosan Nanoparticles and Cation Exchange Resin for the Efficient Purification of Lysine-Tagged Small Ubiquitin-Like Modifier Protease, *J. Chromatogr. B*, **907**: 159–162 (2012).

[21] Chauhan N., Narang J., Pundir C.S., An Amperometric Glutathione Biosensor Based on Chitosan–Iron Coated Gold Nanoparticles Modified Pt Electrode, *Int. J. Biol. Macromol.*, **51(5)**: 879–886 (2012).

[22] Liu L., Xiao L., Zhu H., Shi X., Preparation of Magnetic and Fluorescent Bifunctional Chitosan Nanoparticles for Optical Determination of Copper Ion, *Microchim. Acta*, **178(3–4)**: 413–419 (2012).

[23] Ma W., Ya F.-Q., Han M., Wang R., Characteristics of Equilibrium, Kinetics Studies for Adsorption of Fluoride on Magnetic-Chitosan Particle, *J. Hazard. Mater.*, **143(1)**: 296–302 (2007).

[24] Monier M., Ayad D.M., Abdel-Latif D.A., Adsorption of Cu(II), Cd(II) and Ni(II) ions by Cross-Linked Magnetic Chitosan-2-Aminopyridine Glyoxal Schiff's base, *Colloids Surfaces B Biointerfaces*, **94**: 250–258 (2012).

[25] Maghsoodi V., Mousavi S. M., Rajabi N., Batch Equilibrium and Kinetics Studies of Cd (II) Ion Removal from Aqueous Solution Using Porous Chitosan Hydrogel Beads, *Iran. J. Chem. Chem. Eng. (IJCCE)*, **28(3)**:(2009).

[26] N Oroujzadeh., Rezaei S., Fabrication of a Novel Magnetic Nanocomposite to Remove Cu (II) Ions from Contaminated Water, *Phosphorus. Sulfur. Silicon Relat. Elem.*, (2016).

[27] Wu X., Hu L., Design and Synthesis of Peptide Conjugates of Phosphoramide Mustard as Prodrugs Activated by Prostate-Specific Antigen, *Bioorg. Med. Chem.*, **24(12)**: 2697–2706 (2016).

[28] Jiang Y., Hu L., Peptide Conjugates of 4-Aminocyclophosphamide as Prodrugs of Phosphoramide Mustard for Selective Activation by Prostate-Specific Antigen (PSA), *Bioorg. Med. Chem.*, **21(23)**: 7507–7514 (2013).

[29] Hu L., *et al.*, "Synthesis and Structure–Activity Relationships of Nitrobenzyl Phosphoramide Mustards as Nitroreductase-Activated Prodrugs, *Bioorg. Med. Chem. Lett.*, **21(13)**: 3986–3991 (2011).

[30] Jiang Y., DiPaola R.S., Hu L., Synthesis and Stereochemical Preference of Peptide 4-Aminocyclophosphamide Conjugates As Potential Prodrugs of Phosphoramide Mustard for Activation by Prostate-Specific Antigen (PSA), *Bioorg. Med. Chem. Lett.*, **19(9)**: 2587–2590 (2009).

[31] Gholivand K., Molaei F., Oroujzadeh N., Mobasseri R., Naderi-Manesh H., Two novel Ag (I) Complexes of N-Nicotinyl Phosphoric Triamide Derivatives: Synthesis, X-Ray Crystal Structure and in Vitro Antibacterial and Cytotoxicity Studies, *Inorganica Chim. Acta*, **423**: 107–116 (2014).

[32] Oroujzadeh N., Rezaei S., New Nano Composite of N-Nicotinyl, N′, N ″-Bis (Tert-Butyl) Phosphorictriamide Based on Chitosan: Fabrication and Antibacterial Investigation, *Phosphorus. Sulfur. Silicon Relat. Elem.*, ***191*(11-12)**: 1572-1573 (2016).

[33] Shariatinia Z., Nikfar Z., Synthesis and Antibacterial Activities of Novel Nanocomposite Films of Chitosan/Phosphoramide/Fe_3O_4 NPs, *Int. J. Biol. Macromol.*, **60**: 226–234 (2013).

[34] Omrani R., Ali R.B., Arfaoui Y., Raddaoui A., H Hmani., May M.V El, Akacha A.B., Phosphonoamidates & Phosphopnoamidines: A Convenient Synthesis, Spectroscopic Properties, DFT Calculations & Pharmacological Studies, *Journal of Molecular Structure*, **1236**:130321 (2021).

[35] Gholivand K., Valmoozi A.A.E., Bonsaii M., Synthesis, Biological Evaluation, QSAR Study and Molecular Docking of Novel N-(4-Amino Carbonylpiperazinyl)(Thio) Phosphoramide Derivatives as Cholinesterase Inhibitors, *Pestic. Biochem. Physiol.*, **112**: 40–50 (2014).

[36] Gholivand K., Alizadehgan A.M., Mojahed F., Dehghan G., Mohammadirad A., Abdollahi M., Some New Carbacylamidophosphates as Inhibitors of Acetylcholinesterase and Butyrylcholinesterase, *Zeitschrift für Naturforsch. C*, **63(3–4)**: 241–250 (2008).

[37] Gholivand K., *et al.*, "Acetylcholinesterase Inhibition by Diaza-and Dioxophosphole Compounds: Synthesis and Determination of IC50 Values, *J. Enzyme Inhib. Med. Chem.*, **19(5)**: 403–407 (2004).

[38] Gholivand K., Shariatinia Z., Khajeh K., Naderimanesh H., Syntheses and Spectroscopic Characterization of Some Phosphoramidates as Reversible Inhibitors of Human Acetylcholinesterase and Determination of their Potency, *J. Enzyme Inhib. Med. Chem.*, **21(1)**: 31–35 (2006).

[39] Ruiz M., Sastre A. M., Guibal E., Palladium Sorption on Glutaraldehyde-Crosslinked Chitosan, *React. Funct. Polym.*, **45(3)**: 155–173 (2000).

[40] Ngah W.S.W., Endud C.S., Mayanar R., Removal of Copper (II) Ions from Aqueous Solution Onto Chitosan and Cross-Linked Chitosan Beads, *React. Funct. Polym.*, **50(2)**:181–190 (2002).

[41] Li N., Bai R., Development of Chitosan-Based Granular Adsorbents for Enhanced and Selective Adsorption Performance in Heavy Metal Removal, *Water Sci. Technol.*, **54(10)**: 103–113 (2006).

[42] Martinez L. *et al.*, Cross-Linking of Chitosan and Chitosan/Poly (Ethylene Oxide) Beads: A Theoretical Treatment, *Eur. J. Pharm. Biopharm.*, **67(2)**: 339–348 (2007).

[43] Davarnejad R., Karimi Dastnayi Z., Cd (II) Removal from Aqueous Solutions by Adsorption on Henna and Henna with Chitosan Microparticles Using Response Surface Methodology, *Iran. J. Chem. Chem. Eng. (IJCCE)*, **38(3)**: 267–281, 2019.

[44] Oroujzadeh N., Gholivand K., Jamalabadi N.R., New Carbacylamidophosphates Containing Nicotinamide: Synthesis, Crystallography and Antibacterial Activity, *Polyhedron*, **22**: 29–38 (2017).

[45] Monier M., Ayad D.M., Wei Y., Sarhan A.A., Adsorption of Cu (II), Co (II), and Ni (II) Ions by Modified Magnetic Chitosan Chelating Resin, *J. Hazard. Mater.*, **177(1)**: 962–970 (2010).

[46] Goleij M., Fakhraee H., Response Surface Methodology Optimization of Cobalt (II) and Lead (II) Removal from Aqueous Solution Using MWCNT-Fe_3O_4 Nanocomposite, *Iran. J. Chem. Chem. Eng. (IJCCE)*, **36(5)**: 129–141 (2017).

[47] Chang Y.-C. Chen D.-H., Preparation and Adsorption Properties of Monodisperse Chitosan-Bound Fe_3O_4 Magnetic Nanoparticles for Removal of Cu (II) Ions, *J. Colloid Interface Sci.*, **283(2)**: 446–451 (2005).

[48] Langmuir I., the Constitution and Fundamental Properties of Solids and Liquids. Part i. Solids., *J. Am. Chem. Soc.*, **38(11)**: 2221–2295, 1916.

[49] Freundlich H.M.F., Over the Adsorption in Solution, *J. Phys. Chem*, **57(385471)**: 1100–1107 (1906).

[50] Preetha B. Viruthagiri T., Application of Response Surface Methodology for the Biosorption of Copper Using Rhizopus Arrhizus, *J. Hazard. Mater.*, **143(1):** 506–510 (2007).

[51] Aslan N., Application of Response Surface Methodology and Central Composite Rotatable Design for Modeling the Influence of some Operating Variables of a Multi-Gravity Separator for Coal Cleaning, *Fuel*, **86(5)**: 769–776 (2007).

[52] Davarnejad R., Panahi P., Cu (II) and Ni (II) Removal from Aqueous Solutions by Adsorption on Henna and Optimization of Effective Parameters by Using the Response Surface Methodology, *J. Ind. Eng. Chem.*, **33**: 270–275 (2016).

[53] Dean A., Voss D., Response Surface Methodology, *Des. Anal. Exp.*, 483–529 (1999).

[54] Montgomery D.C., Introduction to Factorial Designs, *Des. Anal. Exp.*, 160–197 (2005).

[55] Khayat Sarkar Z., Khayat Sarkar F., Magnetic Iron Oxide Nanoparticles, Polyethylene Glycol, Surfactant, Superparamagnetic, Chemical Co-Precipitation, *Int. J. Nanosci. Nanotechnol.*, **7(4)**: 197–200 (2011).

[56] Oroujzadeh N., New Chitosan-Silver Nanocomposites Containing N-Nicontinyl Phosphoric Triamide as an Antibacterial-Enhancer Additive, *Iran. J. Chem. Chem. Eng. (IJCCE)*, **39(4)**: 1–9 (2020).

[57] Scherrer P., Bestimmung Der Inneren Struktur und der Größe von Kolloidteilchen Mittels Röntgenstrahlen, "Kolloidchemie Ein Lehrbuch", Springer, 387–409 (1912).

[58] Liu Z., Bai H., Sun D.D., Facile Fabrication of Porous Chitosan/TiO_2/Fe_3O_4 Microspheres with Multifunction for Water Purifications, *New J. Chem.*, **35(1)**: 137–140 (2011).

[59] Dastkhoon M. *et al.*, Ultrasound Assisted Adsorption of Malachite Green dye Onto ZnS: Cu-NP-AC: Equilibrium Isotherms and Kinetic Studies–Response Surface Optimization, *Sep. Purif. Technol.*, **156**: 780–788 (2015).

[60] Huangfu M. *et al.*, Study of the Effect of Absorbed Cu Species on the Surface of Specularite (0 0 1) by the DFT Calculations, *Minerals*, **11(9)**: 930 (2021).

[61] Reddad Z., Gerente C., Andres Y., Le Cloirec P., Adsorption of Several Metal Ions Onto a Low-Cost Biosorbent: Kinetic and Equilibrium Studies, *Environ. Sci. Technol.*, **6(9)**: 2067–2073 (2002).

[62] Tobin J.M., Cooper D.G., Neufeld R. J., Uptake of Metal Ions by Rhizopus Arrhizus Biomass, *Appl. Environ. Microbiol.*, **47(4)**: 821–824 (1984).

[63] Chowdhury S. Saha P., Sea Shell Powder as a New Adsorbent to Remove Basic Green 4 (Malachite Green) from Aqueous Solutions: Equilibrium, Kinetic and Thermodynamic Studies, *Chem. Eng. J.*, **164(1)**: 168–177 (2010).

[64] Li Y., Zeng X., Liu Y., Yan S., Hu Z., Ni Y., Study on the Treatment of Copper-Electroplating Wastewater by Chemical Trapping and Flocculation, *Sep. Purif. Technol.*, **31(1)**: 91–95 (2003).

[65] Blöcher C., Dorda J., Mavrov V., Chmiel H., Lazaridis N.K., Matis K.A., Hybrid Flotation—Membrane Filtration Process for the Removal of Heavy Metal Ions from Wastewater, *Water Res.*, **37(16)**: 4018–4026 (2003).

[66] Mavrov V., Erwe T., Blöcher C., Chmiel H., Study of New Integrated Processes Combining Adsorption, Membrane Separation and Flotation for Heavy Metal Removal from Wastewater, *Desalination*, 1**57(1–3)**: 97–104 (2003).

[67] Juang R.-S., Shiau R.-C., Metal Removal from Aqueous Solutions Using Chitosan-Enhanced Membrane Filtration, *J. Memb. Sci.*, **165(2):**159–167 (2000).

[68] Qdais H.A., Moussa H., Removal of Heavy Metals from Wastewater by Membrane Processes: A Comparative Study, *Desalination*, **164(2)**: 105–110 (2004).

[69] Tünay O., Kabdaşli N.I., Hydroxide Precipitation of Complexed Metals, *Water Res.*, **28(10)**: 2117–2124 (1994).

[70] Monier M., Adsorption of Hg^{2+}, Cu^{2+} and Zn^{2+} Ions from Aqueous Solution Using Formaldehyde Cross-Linked Modified Chitosan–Thioglyceraldehyde Schiff's Base, *Int. J. Biol. Macromol.*, **50(3)**: 773–781, (2012).

[71] Zhu Y., Hu J., Wang J., Competitive Adsorption of Pb (II), Cu (II) and Zn (II) Onto Xanthate-Modified Magnetic Chitosan, *J. Hazard. Mater.*, **221**: 155–161 (2012).

[72] Huang G., Chuo Y., Zhang K., Jeffrey S.H.I., Adsorptive Removal of Copper ions from Aqueous Solution Using Cross-Linked Magnetic Chitosan Beads, *Chinese J. Chem. Eng.*, **17(6)**: 960–966 (2009).

[73] Zhang S., Zhou Y., Nie W., Song L., Zhang T., Preparation of Uniform Magnetic Chitosan Microcapsules and their Application in Adsorbing Copper Ion (II) and Chromium Ion (III), *Ind. Eng. Chem. Res.*, **51(43)**: 14099–14106 (2012).

[74] Zhou Y.-T., Nie H.-L., Branford-White C., He Z.-Y., L.-M. Zhu, Removal of Cu 2+ from Aqueous solution by Chitosan-Coated Magnetic Nanoparticles Modified with α-Ketoglutaric Acid, *J. Colloid Interface Sci.*, **330(1)**: 29–37 (2009).

[75] Monier M., Ayad D.M., Wei Y., Sarhan A.A., Preparation and Characterization of Magnetic Chelating Resin Based on Chitosan for Adsorption of Cu (II), Co (II), and Ni (II) Ions, *React. Funct. Polym.*, **70(4)**: 257–266 (2010).

[76] Cheng T., Chen C., Tang R., Han C.-H., Tian Y., Competitive Adsorption of Cu, Ni, Pb, and Cd from Aqueous Solution Onto fly Ash-Based Linde F (K) Zeolite, *Iran. J. Chem. Chem. Eng. (IJCCE)*, **37(1)**: 61–72 (2018).

[77] Kavitha B., Sarala Thambavani D., Artificial Neural Network Optimization of Adsorption Parameters for Cr (VI), Ni (II) and Cu (II) Ions Removal from Aqueous Solutions by Riverbed Sand, *Iran. J. Chem. Chem. Eng. (IJCCE)*, **39(5)**: 203–223 (2020).

[78] Chubar N., Carvalho J.R., Correia M.J.N., Heavy Metals Biosorption on Cork Biomass: Effect of the Pre-Treatment, *Colloids Surfaces A Physicochem. Eng. Asp.*, **238(1–3)**: 51–58 (2004).

[79] Wu J., Zhang H., Oturan N., Wang Y., Chen L., Oturan M.A., Application of Response Surface Methodology to the Removal of the Antibiotic Tetracycline by Electrochemical Process Using Carbon-Felt Cathode and DSA ($Ti/RuO_2–IrO_2$) Anode, *Chemosphere*, **87(6)**: 614–620 (2012).

[80] Long A., Zhang H., Lei Y., Surfactant Flushing Remediation of Toluene Contaminated Soil: Optimization with Response Surface Methodology and Surfactant Recovery by Selective Oxidation with Sulfate Radicals, *Sep. Purif. Technol.*, **118**: 612–619 (2013).

[81] Xu T., Liu Y., Ge F., Liu L., Ouyang Y., Application of Response Surface Methodology for Optimization of Azocarmine B Removal by Heterogeneous Photo-Fenton Process Using Hydroxy-Iron–Aluminum Pillared Bentonite, *Appl. Surf. Sci.*, **280**: 926–932 (2013).

[82] Zinatizadeh A.A.L., Mohamed A.R., Abdullah A.Z., Mashitah M.D., Isa M.H., Najafpour G.D., Process Modeling and Analysis of Palm Oil Mill Effluent Treatment in an up-flow Anaerobic Sludge Fixed Film Bioreactor Using Response Surface Methodology (RSM), *Water Res.*, **40(17)**: 3193–3208 (2006).

[83] Long A., Lei Y., Zhang H., Degradation of Toluene by a Selective Ferrous Ion Activated Persulfate Oxidation Process, *Ind. Eng. Chem. Res.*, **53(3)**: 1033–1039 (2014).

[84] Qian Q., Mochidzuki K., Fujii T., Sakoda A., Removal of Copper from Aqueous Solution Using Iron-Containing Adsorbents Derived from Methane Fermentation Sludge, *J. Hazard. Mater.*, **172(2)**: 1137–1144 (2009).

[85] El-Ashtoukhy E.-S., Amin N.K., Abdelwahab O., Removal of Lead (II) and Copper (II) from Aqueous Solution Using Pomegranate Peel as a New Adsorbent, *Desalination*, **223(1)**: 162–173 (2008).

[86] Gode F., Atalay E.D., Pehlivan E., Removal of Cr (VI) from Aqueous Solutions Using Modified Red Pine Sawdust, *J. Hazard. Mater.*, **152(3)**: 1201–1207 (2008).

[87] Nadeem R., Hanif M. A., Shaheen F., Perveen S., Zafar M.N., Iqbal T., Physical and Chemical Modification of Distillery Sludge for Pb(II) Biosorption, *J. Hazard. Mater.*, **150(2)**: 335–342, 2008.

[88] Chen Y., Wang J., Removal of Radionuclide Sr^{2+} Ions from Aqueous Solution Using Synthesized Magnetic Chitosan Beads, *Nucl. Eng. Des.*, **242**: 445–451 (2012).